IEEE Photonics Journal
An IEEE Photonics Society Publication

4H–SiC Avalanche Photodiode Linear Array Operating in Geiger Mode

Volume 9, Number 5, October 2017

Lianghui Li
Dong Zhou
Hai Lu
Wenkai Liu
Xiaofan Mo
Fangfang Ren
Dunjun Chen
Ruiqi Wang
Guanglei Li
Rong Zhang
Youdou Zheng

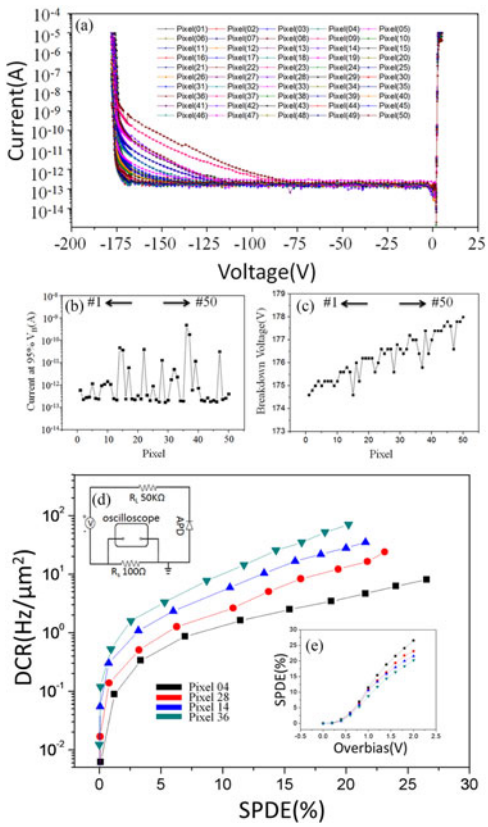

DOI: 10.1109/JPHOT.2017.2750686

4H–SiC Avalanche Photodiode Linear Array Operating in Geiger Mode

Lianghui Li,[1] Dong Zhou,[1] Hai Lu,[1] Wenkai Liu,[1] Xiaofan Mo,[1] Fangfang Ren,[1] Dunjun Chen,[1] Ruiqi Wang,[2] Guanglei Li,[2] Rong Zhang,[1] and Youdou Zheng[1]

[1]School of Electronic Science and Engineering, Collaborative Innovation Center of Advanced Microstructures,Nanjing University, Nanjing 210093, China
[2]State Grid Shandong Electric Power Research Institute, Jinan 250001, China

DOI:10.1109/JPHOT.2017.2750686

Manuscript received July 27, 2017; revised August 28, 2017; accepted September 6, 2017. Date of publication September 11, 2017; date of current version September 19, 2017. This work was supported by the National Key Research and Development Program under Grant 2016YFB0400902. Corresponding author: H. Lu (e-mail: hailu@nju.edu.cn).

Abstract: In this study, a 50-pixel linear array of 4H–SiC ultraviolet avalanche photodiodes operating in Geiger mode is reported for the first time. The 50 pixels within the linear array are all capable of detecting single photons but with a small number of them suffering from extra leakage current near avalanche breakdown. The enhanced leakage is likely correlated with structural defects existing within the epitaxial structure, which would lead to higher dark count rate (DCR) at the same single photon detection efficiency (SPDE) in Geiger mode. For a low-leakage avalanche photodiode device within the linear array, a room temperature SPDE of 15.4% at 280 nm is obtained with a corresponding DCR of 2.5 Hz/μm^2.

Index Terms: 4H-SiC, avalanche photodiodes, linear array, ultraviolet photodetector, Geiger mode.

1. Introduction

During the last two decades, ultraviolet (UV) avalanche photodiodes (APDs) based on 4H-SiC semiconductor have aroused great interest worldwide. When working in Geiger mode, the device has the ability of detecting extremely weak UV signals or even single photons, which has many potential applications such as UV astronomy, environmental monitoring, corona detection, UV lidar, biological detection as well as jet engine or missile plume detection [1], [2]. Compared with traditional vacuum photodetectors, such as photomultiplier tubes (PMTs), SiC APDs have many advantages. They are smaller in size, lower in cost, easier to be integrated and potentially have higher detection efficiency. Besides, semiconductor APDs normally have longer lifetime and can be operated at much lower voltage than that of PMTs. Meanwhile, compared with group-III nitrides, which are also promising wide bandgap semiconductors for UV photodetector applications, currently 4H-SiC semiconductor has considerably lower defect density, which is a key advantage for APD fabrication. As a result, most reported SiC APDs exhibit better performance than their III-nitride counterparts, in terms of dark current, avalanche gain and reliability [3].

Since the first report in 2005, SiC APDs capable of single-photon detection have been demonstrated by several groups worldwide [4]–[6]. Nevertheless, until recently, those studies are mainly focused on discrete APD device and SiC APD linear arrays were less studied [7]–[9]. Moreover, SiC APD linear arrays working in Geiger mode have never been reported, which are urgently

needed for ultra-weak signal detection in emerging UV spectroscopy and imaging applications. The main difficulty in making a workable APD linear array is to achieve a high device yield. Though SiC substrate and epitaxy technologies have gained significant advance in recent years [10], at present commercial SiC wafer still contains many structural defects, which would have remarkable influence on the yield of SiC APDs. For example, if a defect happens to exist within the device active area, which is fairly possible considering the dislocation density of commercial 4H-SiC wafers is around 10^3-10^4 cm^{-2} nowadays and a device area here is assumed as $\sim 10^4$ μm^2, it may cause permanent failure of the APD device before avalanche breakdown. Even if the device doesn't suffer from fatal failure, the defect would degrade the device performance and bring non-uniformity of avalanche characteristics among different devices [11], [12]. In a word, the existence of defects within the device active regions makes successful fabrication of 4H-SiC APD linear arrays difficult. In this work, 4H-SiC APD linear arrays are designed, fabricated and characterized. For the first time, a 50-pixel 4H-SiC APD linear array capable of working in Geiger mode is reported.

2. Experimental Details

As addressed above, material defects have important influence on the yield of 4H-SiC APDs. Thus, the yield issue should be briefly discussed before device fabrication. If the yield of a single APD pixel is defined as Y, since all pixels within a linear array are independent to each other, the yield of the whole linear array (Y_{array}) should be $Y_{array} = Y^N$, where N is the total pixel number of the corresponding APD linear array. Meanwhile, assuming structural defects within 4H-SiC wafer are evenly distributed, then the yield of an APD pixel Y should be described as $Y = e^{-AD}$, where A represents the area of the APD pixel and D represents defect density. Thus, the yield of the linear array can finally be described as $Y_{array} = e^{-ADN}$. There are basically three kinds of material defects in 4H-SiC, which have negative impacts on the performances of APD devices. They are micro-pipes, dislocations and inclusions (3C inclusions for example), respectively [13]–[15]. With the advance of 4H-SiC epitaxial technology, currently micro-pipes and inclusion defects can be nearly eliminated. As a result, dislocations are the main factor to be considered here, which currently have a typical density of 10^3-10^4 cm^{-2}. Again there are three basic types of dislocations in 4H-SiC, which are basal plane dislocation (BPD), threading screw dislocation (TSD) and threading edge dislocation (TED), respectively. Assuming the harmful defect density is 10^3 cm^{-2} in 4H-SiC epi-structure, based on the $Y = e^{-AD}$ equation, when the active area of APD devices is designed to be 1×10^4 μm^2 (100 μm $\times$ 100 μm), the yield of a single APD can be more than 90%. However, if the device area increases to 9×10^4 μm^2 (300 μm $\times$ 300 μm), the yield would drastically drop to 40%. Since the successful fabrication of APD linear arrays relies on high yield of individual pixels, the area of SiC APD pixels is not recommended to exceed 1×10^4 μm^2. The smaller the area is, the higher the yield will be. Meanwhile, if the device area is small, the viewing angle of the linear array would be small too unless large number of pixels are employed, which would also bring down the array yield. As a result of trade-off, the APD pixel size is designed to be 100 μm $\times$ 100 μm in this work.

Fig. 1(a) shows the cross sectional schematic of the 4H-SiC APD pixel. The epitaxial structure is grown on 4-inch n-type substrate, which consists of 10 μm n+ buffer layer ($N_D = 3 \times 10^{18}$ cm^{-3}), a 0.5 μm p- multiplication layer ($N_A = 3 \times 10^{15}$ cm^{-3}), a 0.2 μm p contact layer ($N_A = 2 \times 10^{18}$ cm^{-3}) and 0.15 μm p+ cap layer ($N_A = 3 \times 10^{19}$ cm^{-3}). The device is partially trench isolated to increase device fill factor. The partial trench isolation scheme has been confirmed to be equally effective for suppressing peak electrical field along mesa edge compared with the traditional full trench isolation [16]. Fig. 1(b) and (c) show the top-view images of one APD pixel and the whole 50-pixel APD linear array, respectively. Here it should be noted that the top-view image of Fig. 1(b) is shot before the final pad metal stack are deposited. The purpose is to show the morphology feature that the annealing process causes to the p-metal contact. It is clear that during the ohmic annealing, the p-contact metal stack experiences alloying process and its surface becomes rough.

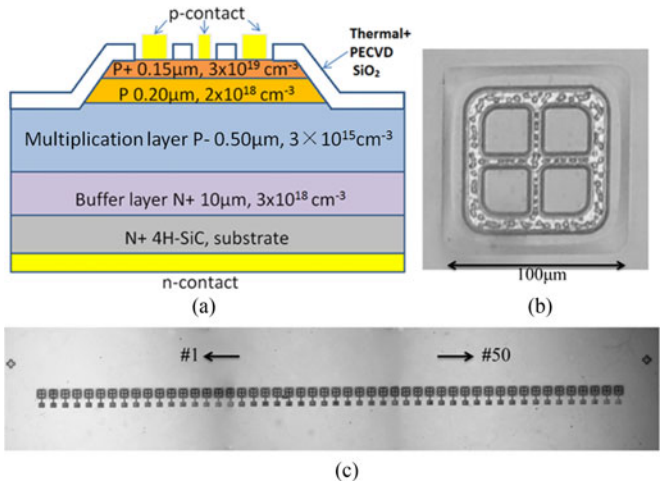

Fig. 1. Cross sectional schematic of the 4H-SiC APD device (a); top-view image of a 4H-SiC APD pixel within the linear array (b); top-view image of a complete 4H-SiC APD linear array (c).

The device fabrication process starts with beveled mesa etching, which is carried out by using an inductively coupled plasma etching system with CF_4/O_2 as the etching gases. By using a photoresist reflow technique, a small bevel angle of $\sim 5°$ is achieved [17]. The device array is then passivated by using thermal oxidation at 1050 °C in dry O_2 atmosphere followed by 1 μm SiO_2 deposition, which is performed by plasma-enhanced chemical vapor deposition at 350 °C. The p-contact windows are opened by using wet chemical etching. Next, n and p contacts both based on Ni/Ti/Al/Au (35 nm/50 nm/150 nm/100 nm) metal stacks are deposited using e-beam evaporation, which are followed by rapid thermal annealing conducted at 850 °C in N_2 atmosphere for 3 min. Finally, the top metal pads based on Ti/Au bi-layer is deposited and patterned by a lift-off process.

3. Results and Discussion

The room temperature (RT) I-V characteristics of the complete set of 50 pixels within the linear array are shown in Fig. 2(a). The dark currents of these devices are all around sub-pA level when the reverse bias is below -75 V. As reverse bias further increases, the majority of the devices still exhibit very low dark current while a few pixels suffer from enhanced leakage current. Nevertheless, the 50 pixels are all capable of having repeatable avalanche breakdown at around 170+ V with maximum avalanche gain up to 10^6. Here, the unity gain is defined at a reverse bias of -75 V.

Fig. 2(b) shows the dark current distribution of the APD devices at their respective 95% breakdown voltage (V_B), which is defined by the reverse voltage when avalanche gain reaches 10^3. It is clear that the dark currents of the 50 pixels vary from 10^{-13} to 10^{-9} A, in which 34 pixels in the linear array do not exhibit early extra leakage current. If these non-leaky devices are regarded as "good" devices, the corresponding device yield is $\sim$68%. The early leakage observed in some devices should be caused by the existence of material defects, especially dislocations within the device active layer. According to previous reports, all dislocations in 4H-SiC would degrade APD performance, while BPDs and TSDs normally cause more extra leakage than TEDs [18]. Thus, based on the yield equation $Y = e^{-AD}$ as discussed above, the dislocation density of the 4H-SiC epi-structure is estimated to be $\sim 3.9 \times 10^3\,\mathrm{cm}^{-2}$, which is within the reasonable range of current SiC material technology.

The V_B of the 50 pixels is sequentially plotted in Fig. 2(c), which varies from 174.6 V to 178.0 V. Interestingly it is found that the V_B increases from pixel No.1 to pixel No.50 in a linear trend. This V_B variation trend from one side to the other side of the linear array is likely caused by small

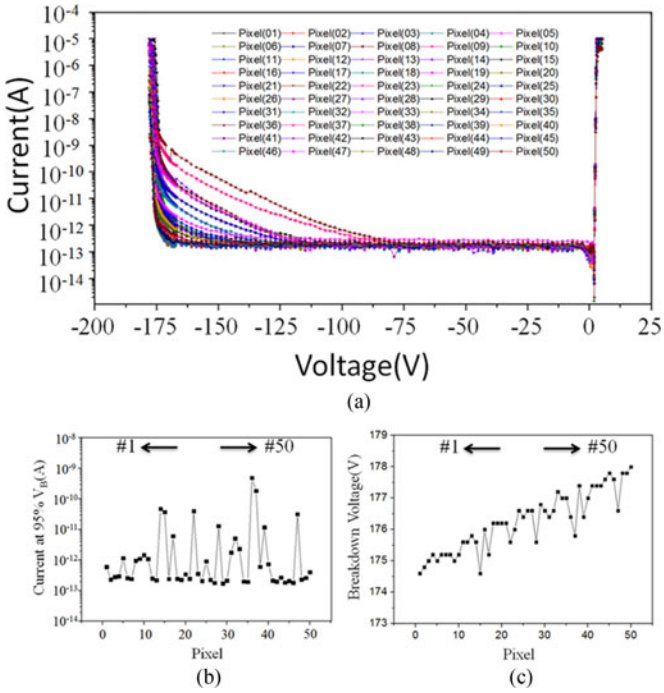

Fig. 2. (a) RT I-V characteristics of the complete 50 pixels within the linear array; (b) distribution of dark currents at 95% breakdown voltage for the 50 pixels; (c) distribution of breakdown voltages for the 50 pixels.

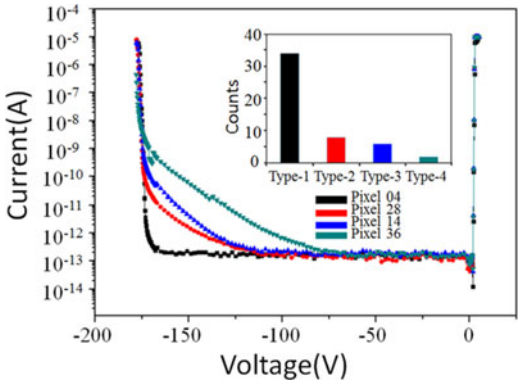

Fig. 3. I-V characteristics of the four APDs representing Type-1 (10^{-13} to 10^{-12} A), Type-2 (10^{-12} to 10^{-11} A), Type-3 (10^{-11} to 10^{-10} A) and Type-4 (10^{-10} to 10^{-9} A) devices, which have different leakage levels; the inset shows the statistical counts of the 4 types of devices.

thickness variation of the p-multiplication layer across the epi-wafer. It has been reported that for InGaAsP/InP single photon counting APDs, an uncertainty of excess bias within 10% requires simultaneous fluctuations in layer thickness and charge density better than 0.5% [19]. Similar requirement on epi-layer uniformity could be also applicable for SiC APDs, which should be the focus of future epitaxy study. Meanwhile, the V_B fluctuation among neighboring devices may be caused by fabrication process or material defects.

Based on the dark current levels at 95% V_B, the 50 pixels within the linear array are divided into 4 groups. As shown in the inset of Fig. 3, 34 of the 50 pixels with dark current in the 10^{-13}–10^{-12} A range is defined as Type-1, 8 pixels with dark current in the 10^{-12}–10^{-11} A range is defined as

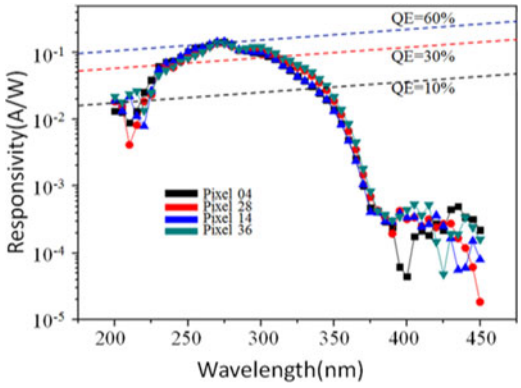

Fig. 4. Spectral response curves of the four representative APDs, which are measured under zero bias.

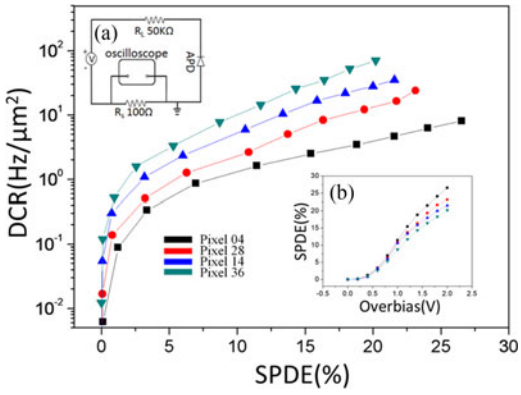

Fig. 5. The RT DCR versus SPDE curves of the four representative APDs; inset (a) shows the passive-quenching circuit used for single photon counting characterization; inset (b) shows the SPDE versus overbias curves of the four representative APDs.

Type-2, 6 pixels with dark current in the 10^{-11}–10^{-10} A range is defined as Type-3, and finally 2 pixels with dark current in the 10^{-10}–10^{-9} A range is defined as Type-4. To study the influence of dark current on other key performance parameters, here the No.4, No.28, No.14 and No.36 pixels are chosen as the representative APD devices of the 4 device types with different dark current levels. The I-V characteristics of the four representative APDs are shown in Fig. 3. It is worth to be noted that the I-V curve of the No.36 pixel is the worst among the whole linear array. The active region of the device is expected to contain larger number of defects or single but most harmful defect.

Fig. 4 shows the spectral response curves of the four representative APDs, which are found basically the same, suggesting that the increase of the APD leakage does not have big influence on their spectral response characteristics. The four APDs exhibit their peak responsivity of ~0.14 A/W at 270 nm, corresponding to a peak quantum efficiency of 63.3%. The UV/visible rejection ratio is $\sim 10^3$, which is defined as the maximum responsivity measured at 270 nm divided by that measured at 400 nm.

Finally, the single photon detection performance of the four representative APDs are compared. As shown in the inset (a) of Fig. 5, the APDs working in Geiger mode are characterized by using a passive quenching circuit [20]. In the experimental setup, the APD device is in series connection with a 50 kΩ quenching resistor (R_L), a DC voltage source and a 100 Ω sampling resistor (R_S), which is further in parallel connection with an oscilloscope or a digital counter. The oscilloscope can record waveform of voltage pulses, while the digital counter is capable of counting the frequency

of voltage pulses. Here the recovery time of the SiC APD in current passive quenching circuit is estimated to be 50∼100 ns [21]. The UV light source used during the test is a 280 nm light emitting diode. The calibrated incident UV photon flux is ∼86 photons/$\mu m^2 \cdot s$.

The RT dark count rate (DCR) versus single photon detection efficiency (SPDE) curves of the four representative APDs are shown in Fig. 5. It is clear that the Type-1 device with the lowest dark current near avalanche breakdown also exhibits the lowest DCR at the same SPDE, while the DCRs of Type-2, Type-3 and Type-4 devices gradually increase, demonstrating an obvious positive correlation between dark current and DCR. It also indicates that the enhanced dark current observed in some APD devices is not surface leakage but true leakage from the pn junction, which would cause parasitic avalanche events. The inset (b) of Fig. 5 shows the SPDE versus overbias (defined as $V\text{-}V_B$) curves of the four representative APDs. At the same overbias, the device having lowest dark current exhibits the highest SPDE, suggesting that those material defects causing dark counts can also lead to photo-carrier loss. For the typical Type-1 APD device that doesn't suffer from early extra leakage current, its RT SPDE at 280 nm is 15.4% with a corresponding DCR of 2.5 Hz/μm^2. Comparatively, for the typical Type-4 device with the highest leakage, its DCR could reach 25.4 Hz/μm^2 at a corresponding SPDE of 14.3%. Here it should be noted that based on the passive quenching scheme used in this work, afterpulsing-induced counts can not be distinguished from real photon counts, which would cause a little bit over-estimation of SPDE at RT. Nevertheless, this limitation would not impact the general trend and comparative results of the SPDE-related curves.

4. Conclusion

In this work, a 50-pixel 4H-SiC APD linear array operating in Geiger mode is successfully demonstrated for the first time. The majority of APD devices within the linear array show sub-pA level dark current at 95% breakdown voltage. Although a few devices do suffer from early extra leakage current, all pixels within the linear array can work in single photon counting mode. For the non-leaky APD pixel, a RT SPDE of 15.4% at 280 nm is obtained with a corresponding DCR of 2.5 Hz/μm^2. A positive correlation between early extra leakage and DCR is observed. This study indicates that besides further reducing defect density within the epi-structure, tight control of uniformity in terms of multiplication layer thickness and doping density is also very important for the future implementation of 4H-SiC single photon counting UV imaging arrays.

References

[1] F. Yan, Y. Luo, J. H. Zhao, and G. H. Olsen, "4H-SiC visible blind UV avalanche photodiodes," *Electron. Lett.*, vol. 35, no. 11, pp. 929–930, 1999.
[2] J. C. Campbell *et al.*, "Recent advances in avalanche photodiodes," *IEEE J. Sel. Topics Quantum Electron*, vol. 10, no. 4, pp. 777–787, Jul./Aug. 2004.
[3] B. Yang, A. L. Beck, R. D. Dupuis, and J. C. Campbell, "GaN avalanche photodiodes," *Appl. Phys. Lett.*, vol. 76, no. 7, pp. 924–926, 2000.
[4] X. Xin *et al.*, "Demonstration of 4H-SiC UV single photon counting avalanche photodiode," *Electron. Lett.*, vol. 41, no. 4, pp. 212–214, 2005.
[5] A. L. Beck, G. Karve, S. Wang, J. Ming, X. Guo, and J. C. Campbell, "Geiger mode operation of ultraviolet 4H-SiC avalanche photodiodes," *IEEE Photon. Technol. Lett.*, vol. 17, no. 7, pp. 1507–1509, Jul. 2005.
[6] A. Vert, S. Soloviev, J. Fronheiser, and P. Sandvik, "Solar-blind 4H-SiC single-photon avalanche diode operating in Geiger mode," *IEEE Photon. Technol. Lett.*, vol. 20, no. 18, pp. 1587–1589, Sep. 2008.
[7] F Yan *et al.*, "Demonstration of 4H-SiC avalanche photodiodes linear array," *Solid-State Electron.*, vol. 47, no. 2, pp. 241–245, 2003.
[8] G. A. Shaw *et al.*, "Deep UV photon-counting detectors and applications," *Proc. SPIE*, vol. 7320, pp. 73200J1–73200J15, 2009.
[9] P. Sandvik, S. Soloviev, A. Vert, A. Bolotnikov, J. McMahon, and J. Campbell, "SiC deep ultraviolet avalanche photodetectors," Gen. Electr. Global Res., Niskayuna, NY, USA, Tech. Rep. W911NF-06-C-0160, 2010.
[10] B. L. VanMil, R. E. Stahlbush, R. L. Myers-Ward, K.-K. Lew, C. R. Eddy, Jr., and D. K. Gaskill, "Basal plane dislocation reduction for 8° off-cut, 4H-SiC using in situ variable temperature growth interruptions," *J. Vac. Sci. Technol. B, Microelectron. Nanometer Struct.*, vol. 26, no. 4, pp. 1504–1507, 2008.

[11] R. A. Berechman, M. Skowronski, S. Soloviev, and P. Sandvik, "Electrical characterization of 4H–SiC avalanche photodiodes containing threading edge and screw dislocations," *J. Appl. Phys.*, vol. 107, no. 11, pp. 114504-1–114504-4, 2010.
[12] A. V. Vert, S. I. Soloviev, J. Fronheiser, and P. M. Sandvik, "Influence of defects in 4H-SiC avalanche photodiodes on Geiger-mode dark count probability," *Mater. Sci. Forum*, vols. 615–617, pp. 877–880, 2009.
[13] P. G. Neudeck and J. A. Powell, "Performance limiting micropipe defects in silicon carbide wafers," *IEEE Electron Device Lett.*, vol. 15, no. 2, pp. 63–65, Feb. 1994.
[14] P. G. Neudeck, W. Huang, and M. Dudley, "Study of bulk and elementary screw dislocation assisted reverse breakdown in low-voltage ($<$250 V) 4H-SiC p($+$)n junction diodes—Part I: DC properties," *IEEE Trans. Electron. Devices*, vol. 46, no. 3, pp. 478–484, Mar. 1999.
[15] T. Kimoto, N. Miyamoto, and H. Matsunami, "Performance limiting surface defects in SiC epitaxial p-n junction diodes," *IEEE Trans Electron Devices*, vol. 46, no. 3, pp. 471–477, Mar. 1999.
[16] L. Li, "High fill-factor 4H-SiC avalanche photodiodes with partial trench isolation," *IEEE Photon. Technol. Lett.*, vol. 28, no. 22, pp. 2526–2528, Nov. 2016.
[17] D. Zhou *et al.*, "High-temperature single photon detection performance of 4H-SiC avalanche photodiodes," *IEEE Photon. Technol. Lett.*, vol. 26, no. 11, pp. 1136–1138, Jun. 2014.
[18] A. Grekov, Q. Zhang, H. Fatima, A. Agarwal, and T. Sudarshan, "Effect of crystallographic defects on the reverse performance of 4H-SiC JBS diodes," *Microelectron. Rel.*, vol. 48, no. 10, pp. 1664–1668, 2008.
[19] H.-Z. Song, J. Deng, Q. Dai, Z. Shi, and L.-B. Yu, "Quantitative correlation between fabrication precision and device homogeneity of single-photon avalanche diodes," *IEEE Trans. Electron Devices*, vol. 63, no. 12, pp. 4845–4851, Dec. 2016.
[20] H. Dautet *et al.*, "Photon counting techniques with silicon avalanche photodiodes," *Appl. Opt.*, vol. 32, no. 21, pp. 3894–3900, 1993.
[21] S. Cova, M. Ghioni, A. Lacaita, C. Samori, and F. Zappa, "Avalanche photodiodes and quenching circuits for single-photon detection," *Appl. Opt.*, vol. 35, no. 12, pp. 1956–1976, 1996.